Modeling the thermal conductivities of the zinc antimonides ZnSb and Zn_4Sb_3

Lasse Bjerg and Bo B. Iversen
Center for Materials Crystallography, Department of Chemistry and iNANO, Aarhus University, Denmark

Georg K. H. Madsen*
Department of Atomistic Modelling and Simulation, ICAMS, Ruhr-Univesität Bochum, Germany
(Received 20 July 2013; revised manuscript received 13 December 2013; published 13 January 2014)

ZnSb and Zn_4Sb_3 are interesting as thermoelectric materials because of their low cost and low thermal conductivity. We introduce a model of the lattice thermal conductivity which is independent of fitting parameters and takes the full phonon dispersions into account. The model is found to give thermal conductivities with the correct relative magnitudes and in reasonable quantitative agreement with experiment for a number of semiconductor structures. The thermal conductivities of the zinc antimonides are reviewed and the relatively large effect of nanostructuring on the zinc antimonides is rationalized in terms of the mean free paths of the heat carrying phonons. The very low thermal conductivity of Zn_4Sb_3 is found to be intrinsic to the structure. However, the low-lying optical modes are observed in both Zn-Sb structures and involve both Zn and Sb vibrations, thereby strongly questioning dumbbell rattling. A mechanism for the very low thermal conductivity observed in Zn_4Sb_3 is identified. The large Grüneisen parameter of this compound is traced to the Sb atoms which coordinate only Zn atoms.

DOI: 10.1103/PhysRevB.89.024304 PACS number(s): 63.20.dk, 63.20.Ry, 66.70.Df

I. INTRODUCTION

Thermoelectric materials are capable of interconverting heat and electricity. As for any heat engine, the conversion efficiency is limited by the Carnot efficiency. Moreover, the dimensionless figure of merit of a material is limiting,

$$zT = \frac{S^2\sigma}{\kappa_e + \kappa_l}T, \tag{1}$$

where S is the Seebeck coefficient, σ is the electric conductivity, κ_e and κ_l are the electric and lattice thermal conductivities, and T is the temperature. Generally, a zT above 1 is needed for sufficient conversion efficiency.

Besides having a high zT, a good thermoelectric material should be made from abundant and nontoxic components. For this reason, Zn and Sb based compounds have attracted interest. Zn_4Sb_3 first gained interest because of it having a lattice thermal conductivity of just 0.6 W m^{-1} K^{-1} at room temperature, whereby zT values above 1 were obtained [1]. Though progress has been made in increasing its stability [2–4], the inherent instability of Zn_4Sb_3, which decomposes into ZnSb, Sb, and ZnO upon cycling in air [2,5,6], has increased the interest in ZnSb as a thermoelectric material [7–16]. At room temperature, single crystalline ZnSb has been found to have a thermal conductivity of 3–4 W m^{-1} K^{-1} [17], and for polycrystalline and doped samples, values below 2 W m^{-1} K^{-1} have been obtained [7,8,11,12,16]. A zT of 0.9 at 550 K has been reported [7,12].

Based on the observation of abundant Zn vacancies and interstitials, the low thermal conductivity of Zn_4Sb_3 has been attributed to the high crystalline disorder of Zn_4Sb_3 [18–20]. A different interpretation related the low thermal conductivity to an observed low-lying optical phonon which was attributed to Sb-Sb dumbbell rattling [21]. However, these mechanisms were both conjectures and only limited quantitative models have been introduced for the thermal conductivity.

Probably, the simplest models with quantitatively predictive power are based on Klemens-Callaway models of the Debye solid. While such simple models cannot be expected to reach the same precision as a solution of the full Boltzmann transport equation [22,23], they have been found to give the correct order of magnitude for the thermal conductivity over a surprising large range of solids [24]. They are, hence, well suited for quantifying a discussion of the structural origins of a "low" thermal conductivity, as seen, e.g., in a discussion of the influence of lone pairs on the thermal conductivity [25]. Furthermore, their computational simplicity makes them interesting in their own right in, e.g., a high-throughput framework where they can provide a first estimate of thermal conductivity. The aim of the present paper is thus twofold. First of all, we take a step beyond earlier *ab initio* based models, which take only the linear part of the acoustic bands into account [26], by integrating over the full set of group velocities, thereby taking the information available from *ab initio* calculations better into account. We validate the model by showing how it can reliably reproduce the ordering of the measured thermal conductivities in a number of compounds, including the structurally complex zinc antimonides.

In the second part, we investigate the origins of the low thermal conductivity of ZnSb and Zn_4Sb_3. The thermal conductivities of the zinc antimonides are reviewed and it is shown that to explain the observed thermal conductivities, grain boundary and impurity scattering must be introduced. However, it is also found that the very low thermal conductivity of Zn_4Sb_3 is inherent of the structure. The low-frequency optical peaks in both Zn-Sb compounds can be attributed to cooperative Zn and Sb motion, questioning dumbbell rattling. On the contrary the low thermal conductivity is related to an exceptionally large squared Grüneisen parameter and it is shown how it originates from anharmonic vibration of the Sb atoms which are not bonded in dumbbells.

*georg.madsen@rub.de

II. BACKGROUND

Within the relaxation-time approximation, the lattice thermal conductivity is given as

$$\kappa_l(T) = \frac{1}{3}\sum_i \int \frac{d\mathbf{q}}{8\pi^3} v_{i\mathbf{q}}^2 \tau_{i\mathbf{q}} C_{i\mathbf{q}}, \tag{2}$$

where the sum is over all phonon bands; the integral is over all q points in the first Brillouin zone; $v_{i\mathbf{q}}$ is the group velocity of a given phonon mode; $\tau_{i\mathbf{q}}$ is the mode relaxation time; and $C_{i\mathbf{q}}$ is the mode heat capacity depending only on the mode frequency $\omega_{i\mathbf{q}}$ and the temperature.

Except for the relaxation time, the quantities in Eq. (2) can be extracted directly from the phonon dispersion relation of a material. The relaxation-time model used in this paper is based on the model of three-phonon anharmonic scattering developed by Slack and co-workers [24,27,28]. There are, at least, two different models in the literature. One is based on the empirical finding that a good expression for the relaxation time around the Debye temperature θ_D is [27,28]

$$\tau_{\mathrm{M}}^{-1} = p\omega^2 \frac{T}{\theta_D} e^{-\theta_D/3T}. \tag{3}$$

A somewhat different model was given by Slack [24] based on work on noble gas crystals by Leibfried and Schlömann [29], and Julian [30],

$$\kappa_l^{\mathrm{Slack}}(\theta_D) = \frac{0.849 \times 3\sqrt[3]{4}}{20\pi^3(1 - 0.514\gamma^{-1} + 0.228\gamma^{-2})} \times \left(\frac{k_B\theta_D}{\hbar}\right)^2 \frac{k_B M V^{1/3}}{\hbar\gamma^2}, \tag{4}$$

where γ is the Grüneisen parameter, V is the unit cell volume of and M is the average atomic mass.

The two models can be compared by considering a Debye model where all three branches have the same sound speed s, relaxation time, and Debye temperature, where Eq. (2) gives

$$\kappa_l^{\mathrm{Debye}}(T) = \frac{k_B}{2\pi^2 s}\left(\frac{k_B T}{\hbar}\right)^3 \int_0^{\theta_D/T} \tau \frac{x^4 e^x dx}{(e^x - 1)^2}. \tag{5}$$

By inserting Eq. (3) in Eq. (5) and evaluating the thermal conductivity at the Debye temperature

$$\kappa_l(\theta_D) = p^{-1}\frac{k_B^2\theta_D\sqrt[3]{e}}{2\pi^2 s\hbar}\int_0^1 \frac{x^2 e^x dx}{(e^x - 1)^2}. \tag{6}$$

If we equate Eqs. (6) and (4), we obtain

$$p = \frac{1 - 0.514\gamma^{-1} + 0.228\gamma^{-2}}{0.0948}\frac{\hbar^2\gamma^2}{k_B\theta_D M V^{1/3} s}. \tag{7}$$

Inserting a Debye temperature of

$$\theta_D = \sqrt[3]{6\pi^2}\frac{\hbar s}{k_B} \tag{8}$$

into Eq. (7), for ordinary γ values between 0.6 and 1.8, we get the expression

$$p \approx 2\frac{\hbar\gamma^2}{M s^2}. \tag{9}$$

This is double the value used elsewhere in the literature [27,28]. The factor of 2 was discovered by Julian [30] as a correction to Leibfried and Schlömann's expression [29].

The idea behind the present model is to take the full *ab initio* calculated phonon dispersion into consideration when evaluating Eq. (2), but to replace $\tau_{i\mathbf{q}}$ by an ω and T dependent model τ, given by Eqs. (3) and (7). Based on the discussion by Slack we use different definitions of the Debye temperature and Grüneisen parameters [24]. The Debye temperature is obtained from the second moment of the whole phonon spectrum

$$\tilde{\theta}_D = n^{-1/3}\sqrt{\frac{5\hbar^2}{3k_{\mathrm{B}}^2}\frac{\int_0^\infty \omega^2 g(\omega)d\omega}{\int_0^\infty g(\omega)d\omega}}, \tag{10}$$

where n is atoms per unit cell. The overall Grüneisen parameter is defined as

$$\gamma = \frac{\sum_i \int \frac{d\mathbf{q}}{8\pi^3}\gamma_{i\mathbf{q}} C_{i\mathbf{q}}}{\sum_i \int \frac{d\mathbf{q}}{8\pi^3} C_{i\mathbf{q}}}, \qquad \gamma_{i\mathbf{q}} = -\frac{V}{\omega_{i\mathbf{q}}}\frac{\partial\omega_{i\mathbf{q}}}{\partial V}, \tag{11}$$

and is directly related to the observable thermal expansion coefficient. In Slack's model, the sum over the squared Grüneisen parameter is used, thereby avoiding a cancellation between the acoustic modes, which can have a negative Grüneisen parameter, and the optical modes

$$\tilde{\gamma}^2 = \frac{\sum_i \int \frac{d\mathbf{q}}{8\pi^3}\gamma_{i\mathbf{q}}^2 C_{i\mathbf{q}}}{\sum_i \int \frac{d\mathbf{q}}{8\pi^3} C_{i\mathbf{q}}}. \tag{12}$$

Furthermore, since mainly the acoustic bands contribute to the thermal conductivity, the sum is be performed only over modes having an energy less than $k_{\mathrm{B}}\tilde{\theta}_D$.

The model gives a fitting-parameter-free expression for calculating the thermal conductivity of a material. It has the advantage that it takes the full phonon band structure into account when evaluating the mean velocities. Furthermore, $\tilde{\gamma}^2$, s, and $\tilde{\theta}_D$ can be evaluated quite straightforwardly from the phonon band structure, thereby avoiding a certain arbitrariness in making a Debye model for a given solid.

Using this model, and the computational methods described in the next section, we have calculated the lattice thermal conductivity κ_l^{M} of four reference compounds Si, Mg_2Si, ZnTe, and CdTe and the zinc antimonides ZnSb and Zn_6Sb_5 at 300 K (Table I). We compare the values obtained using our model to those of a simpler model given by Slack

$$\kappa_l^{\mathrm{Slack}}(T) = \kappa_l^{\mathrm{Slack}}(\theta_D)\frac{\theta_D}{T}. \tag{13}$$

The factor θ_D/T is introduced to comply with the observed T^{-1} behavior of the thermal conductivity at temperatures above the Debye temperature [24]. Both models are found to predict the right order of magnitude of the thermal conductivities (Table I). For all compounds, the Slack model predicted the highest κ values and the present model is found to give results in better agreement with experiment. Shown in Fig. 1 is the relative thermal conductivity with respect to mean free path for Si and Mg_2Si compared to literature data obtained using the full Boltzmann transport equation [31,32]. It is seen that good agreement is obtained, further lending credibility to the model.

TABLE I. Calculated average sound velocity, Eq. (19); Grüneisen parameter, Eq. (12); reduced Debye temperature, Eq. (10); $\omega^2\tau_{\rm M}$; and $\overline{(v/\omega)^2}$. The thermal conductivity calculated using Eqs. (2), (3), and (7), $\kappa_l^{\rm M}$, Eq. (13), $\kappa_l^{\rm Slack}$, and experiment, $\kappa_l^{\rm Expt.}$, at 300 K are also reported.

Compound	s (m/s)	$\tilde{\gamma}^2$	$\tilde{\theta}_D$ (K)	$(\omega^2\tau_{\rm M})$ 10^{15} s^{-1}	$\overline{(v/\omega)^2}$ 10^{-15}J m^{-1} K^{-1}	$\kappa_l^{\rm M}$ (W m^{-1} K^{-1})	$\kappa_l^{\rm Slack}$ (W m^{-1} K^{-1})	$\kappa_l^{\rm Exp}$ (W m^{-1} K^{-1})
Si	5260	0.66	521	33.8	5.9	200	234	157 [33]
Mg_2Si	5318	1.39	296	3.5	4.2	15	17	11 [20]
ZnTe	2413	0.62	194	6.1	4.0	25	49	18 [34]
CdTe	1952	1.00	155	2.5	3.6	9	21	8 [34]
ZnSb	2241	0.58	92	2.3	2.9	6.6	10.6	3.5 [8]
Zn_6Sb_5	1805	2.59	77	0.3	2.3	0.7	1.4	0.5-1.4 [35,36]

To understand the different results obtained using our method and Slack's method, we can take $\omega^2\tau_{\rm M}$ out of the integral in Eq. (2), and change the integral to a frequency integral over a velocity density of states, g_{v^2},

$$\kappa_l^{\rm M}(T) = (\omega^2\tau_{\rm M})\overline{(v/\omega)^2} \tag{14}$$

with

$$\overline{(v/\omega)^2} = \int_0^\infty g_{v^2}(\omega)\frac{C(\omega)}{\omega^2}d\omega, \tag{15}$$

$$g_{v^2}(\omega) = \frac{1}{3}\sum_i \int \frac{d\mathbf{q}}{8\pi^3} v_{i\mathbf{q}}^2 \delta(\omega - \omega_{i\mathbf{q}}), \tag{16}$$

where δ is the Dirac delta function. In Fig. 2, the density of states g is shown together with g_{v^2} and $g_{v^2}C/\omega^2$ for ZnTe and ZnSb. Clearly, the acoustic modes give the largest contribution to $\kappa_l^{\rm M}$, but the lowest optic branches cannot be neglected. The Debye model is depicted by the dashed line in Fig. 2. For a Debye solid, $g_{v^2}C/\omega^2 = C/(2\pi^2 s)$ up to an energy of $k_{\rm B}\tilde{\theta}_D$. As C is almost ω independent at $T = 300$ K, this corresponds to an almost square area. $\kappa_l^{\rm Slack}$ corresponds to taking the integral under the dashed curve, and we found that the simpler method in all cases gave a too big integral. Furthermore, both $(\omega^2\tau_{\rm M})$ and $\overline{(v/\omega)^2}$ are only weakly temperature dependent above the Debye temperature and can thus be viewed as materials dependent constants. They are listed in Table I and will be used to quantify the discussion of the thermal conductivity in the following.

III. COMPUTATIONAL METHODS

Since Zn_4Sb_3 is highly disordered, a somewhat representative unit cell is very large. Therefore, we performed calculations on the ordered, interstitial-free Zn_6Sb_5 unit cell. The difference between the structures is given in Table II. A force-constant matrix was obtained with the finite-displacements method in $2 \times 2 \times 2$ supercells. The forces were calculated using density functional theory as implemented in VASP [37,38]. From this, the dynamical matrix can be found and diagonalized to obtain the phonon mode eigenvectors and eigenfrequencies. We used the Perdew-Burke-Ernzerhof (PBE) functional [39] with projector augmented wave basis sets [40,41] and a cut-off energy of 360 eV. For ZnSb, we used a $6 \times 5 \times 5$ k grid, whereas a $4 \times 4 \times 4$ k grid was used for Zn_6Sb_5.

We calculated the phonon dispersion relation using PHONOPY [42]. The phonon modes were calculated on a $32 \times 26 \times 24$ q grid for ZnSb and a $32 \times 32 \times 32$ q grid for Zn_6Sb_5. The integrals, Eqs. (2), (10), and (12), were calculated using a histogram method and are converged at the given grids. We repeated this procedure for unit cell volumes which were $\pm 3\%$ of the relaxed volume. For the changed volumes, the atomic positions were relaxed, and the lattice constants were allowed to change while keeping the unit-cell volume constant.

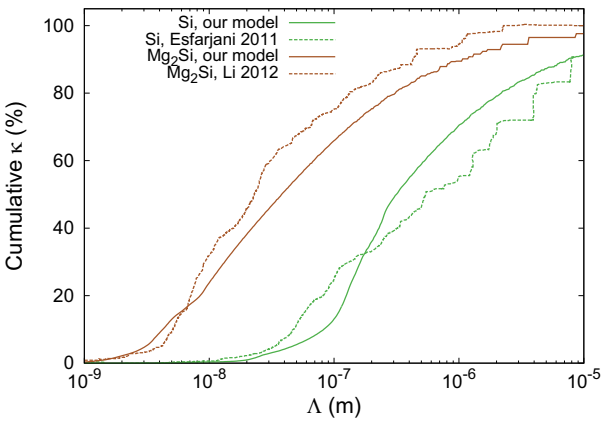

FIG. 1. (Color online) Calculated cumulative thermal conductivity as a function of mode mean free path for Si and Mg_2Si at 300 K compared to literature data calculated using the full Boltzmann equation [31,32].

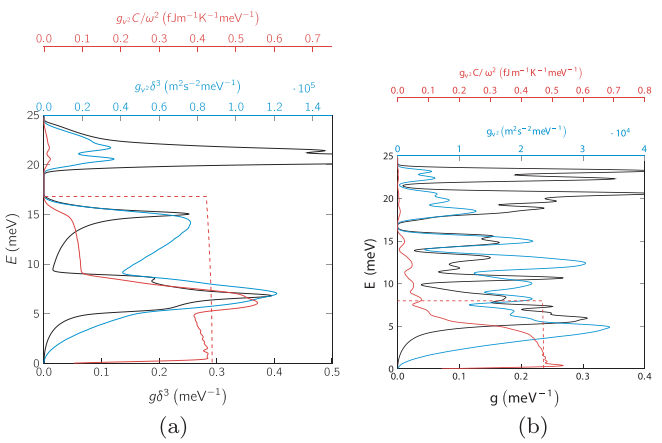

FIG. 2. (Color online) g, g_{v^2}, and $g_{v^2}C/\omega^2$ for (a) ZnTe and (b) ZnSb. Also shown with a dashed line is $g_{v^2}C/\omega^2$ for a Debye model. C is evaluated at $T = 300$ K and is almost ω independent.

TABLE II. Comparison of the experimental structure Zn_4Sb_3 [18], and the theoretical structure Zn_6Sb_5. Zn_4Sb_3, furthermore, contains three interstitial sites with 5%–6% occupancy.

Atom	Parameter	Zn_4Sb_3	Zn_6Sb_5
	Space group	$R\bar{3}c$	$R\bar{3}c$
	a	12.2282	12.3310
	c	12.4067	12.3011
Zn1	x	0.0792	0.0813
	y	0.2439	0.2432
	z	0.4033	0.4023
	Occupancy	0.8999	1
Sb1	x	0.3555	0.3564
	y	0	0
	z	0.25	0.25
	Occupancy	1	1
Sb2	x	0	0
	y	0	0
	z	0.1364	0.1347
	Occupancy	1	1

The velocities and Grüneisen parameters are calculated using the phonon eigenvectors $e_{i\mathbf{q}}$:

$$v_{i\mathbf{q}} = \frac{1}{2\omega_{i\mathbf{q}}}\langle e_{i\mathbf{q}}|\frac{\partial D}{\partial \mathbf{q}}|e_{i\mathbf{q}}\rangle, \tag{17}$$

$$\gamma_{i\mathbf{q}} = -\frac{V}{2\omega_{i\mathbf{q}}^2}\langle e_{i\mathbf{q}}|\frac{\partial D}{\partial V}|e_{i\mathbf{q}}\rangle. \tag{18}$$

Volume changes of $\pm 1\%$ were also tested and the results changed only little. To determine s, a spatial average of v close to the Γ point was taken for each acoustic branch. Then, an average was taken over the three acoustic bands

$$s = \left(\frac{1}{3}\sum_{i=1}^{3}\frac{1}{s_i^3}\right)^{-1/3}. \tag{19}$$

IV. RESULTS AND DISCUSSION

Experimentally measured thermal conductivities can be strongly sample dependent, and it can be necessary to consider the contributions of grain boundaries and defects to the scattering of the heat carrying phonons in order to understand the low thermal conductivity. At the same time Table I shows good overall agreement between the model and experiment without including such effects. This is even the case for the ordered 6:5 model of the Zn_4Sb_3 structure, which would indicate that the low thermal conductivity is inherent of the structure. The discussion is thus split into a quantitative comparison with experiment and a more qualitative discussion of the origin of the low thermal conductivity in Zn_4Sb_3.

A. Thermal conductivity of the zinc antimonides

For the present comparison we write the resistive relaxation time as

$$\tau^{-1} = \tau_{\mathrm{M}}^{-1} + \tau_{\mathrm{B}}^{-1} + \tau_{\mathrm{V}}^{-1}. \tag{20}$$

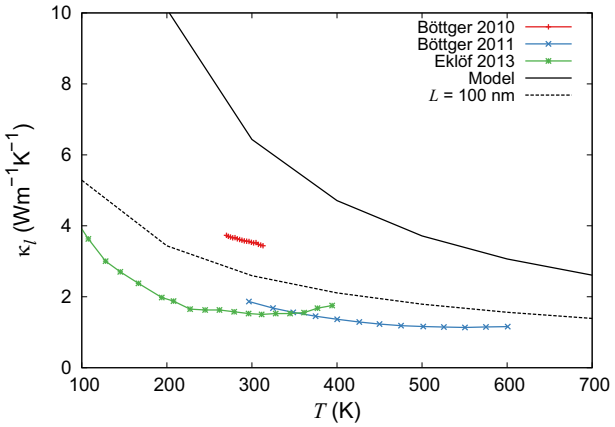

FIG. 3. (Color online) Calculated and experimental [8,11,16] thermal conductivity of ZnSb. The first sample was unprocessed, whereas the latter two were ball milled and ground, respectively. Little anisotropy was found in the calculated values, which are shown as averages over the x, y, and z directions.

Here, we have taken boundary (B) and vacancy (V) scattering into account. For a crystallite with shortest dimension L, it is normally assumed that the boundary scattering relaxation time is [43]

$$\tau_{\mathrm{B}}^{-1} = v/L. \tag{21}$$

A vacancy (V) will give rise to a mass difference equal to the mass of the missing atom, M_V. Furthermore, the breaking of bonds will contribute in a way corresponding to a mass difference of $2M$. This will cause a relaxation time from vacancies of [44]

$$\tau_{\mathrm{V}}^{-1} = c\left(\frac{M_V}{M}+2\right)^2\frac{V\omega^4}{4\pi n s^3}, \tag{22}$$

where c is the vacancy concentration.

Figure 3 shows the calculated thermal conductivity as a function of the temperature for ZnSb compared to experimental measurements. Few reports have been made on measurements of the thermal conductivity of ZnSb single crystals. In 1966 Shaver and Blair reported a value of

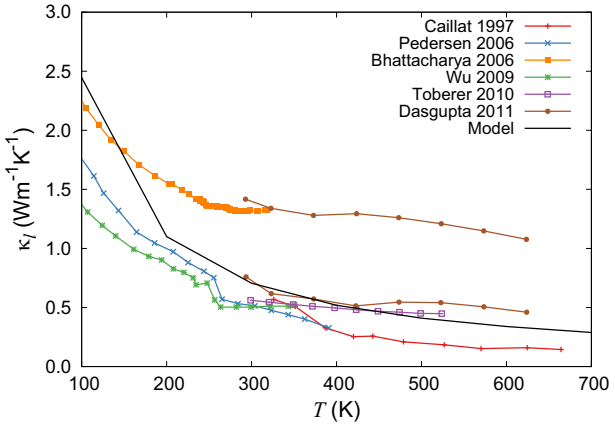

FIG. 4. (Color online) Calculated and experimental [1,35,36,46–48] thermal conductivity of Zn_6Sb_5.

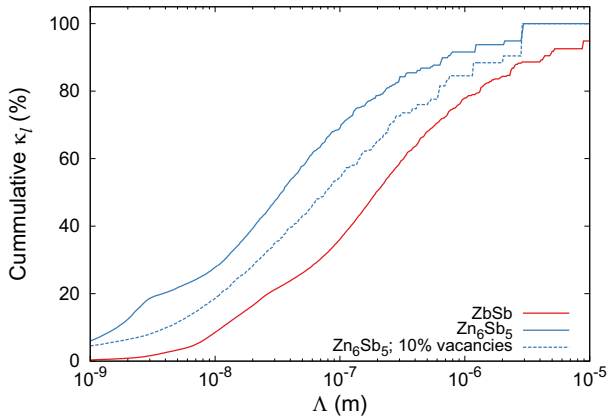

FIG. 5. (Color online) Cumulative thermal conductivity as a function of mode mean free path for ZnSb and Zn_6Sb_5 at 300 K.

3.5 W m^{-1} K^{-1} at room temperature [17]. This value was also found by Böttger *et al.* in 2010 on a polycrystalline sample [8]. Other experiments show a considerably lower thermal conductivity. Böttger *et al.* reported on ball-milled samples in 2011 [11], and Eklöf *et al.* on ground samples in 2013 [16]. Both groups reported values below 2 W m^{-1} K^{-1}. All reported thermal conductivities are the right order of magnitude, but lower than our calculated values. The lower thermal conductivities might arise from smaller grain sizes and less dense samples, and Fig. 3 illustrates how including a boundary scattering based on $L = 100$ nm, Eq. (21), leads to a thermal conductivity in good agreement with experiment.

In Fig. 4, a review of the measured thermal conductivities for Zn_4Sb_3 is shown. Battacharya *et al.* [36] did not observe a drop in the thermal conductivity at 250 K, where an order-disorder phase transition of the Zn sublattice in Zn_4Sb_3 occurs [45]. Schweika *et al.* used the absence of this drop to rule out a dominant role from Zn disorder on the thermal conductivity [21]. However, this argument overlooked the measurements by Pedersen *et al.* [35], which were also available at the time, and show a drop in the thermal conductivity at 250 K. This drop was later confirmed by measurements by Wu *et al.* [46]. It is also clear that the samples not exhibiting a drop at 250 K have a higher thermal conductivity than the ones that do. The discrepancy between these results agrees well with the study by Dasgupta *et al.* [47] who performed a systematic study of synthesis conditions and their effect on the transport properties [47]. It was found that Zn-depleted Zn_4Sb_3 has a thermal conductivity more than double that of more Zn-rich samples. The measurements were only performed above room temperature, but it is seen (Fig. 4), that the thermal conductivity of the Zn-depleted phases agree well with the results where no drop at 250 K is observed, whereas Zn-rich samples agree with the low thermal conductivity observed for samples which have a drop at 250 K.

Figure 4 shows that the calculated thermal conductivity is in good agreement with experiment. Considering the simplicity of the model and the complexity of the real Zn_4Sb_3 structure, the agreement is probably somewhat fortuitous. However, the general ability of the model to predict the relative magnitudes of the thermal conductivities is again validated. It would thus appear that the low thermal conductivity of Zn_4Sb_3 is indeed related to the structure itself. To get an estimate of the role of defects in lowering the thermal conductivity of Zn_4Sb_3, we included scattering from the experimentally observed 10% Zn vacancies [18] through Eq. (22). At 300 K this resulted in a 47% reduction of κ.

In order to predict the effect of microstructuring on the thermal conductivity, we calculated the cumulative contributions to κ as a function of phonon mean free path (MFP)

$$\Lambda = \tau v. \tag{23}$$

The results are shown in Fig. 5. It is seen that the main heat carrying phonons have MFPs between 10 and 1000 nm. This disagrees with the model of Schweika *et al.* [21] which estimated an extremely low MFP of the heat carrying phonons of 0.96 nm. The difference in MFP has important implications for the effect of nanostructuring. At 300 K, 64% of the heat in ZnSb is carried by phonons with a mean free path longer than 100 nm, whereas the same is true for 42% of the heat at 800 K, which explains the large effect of nanostructuring (Fig. 3). Figure 5 also shows the MFP of Zn_6Sb_5. It is interesting

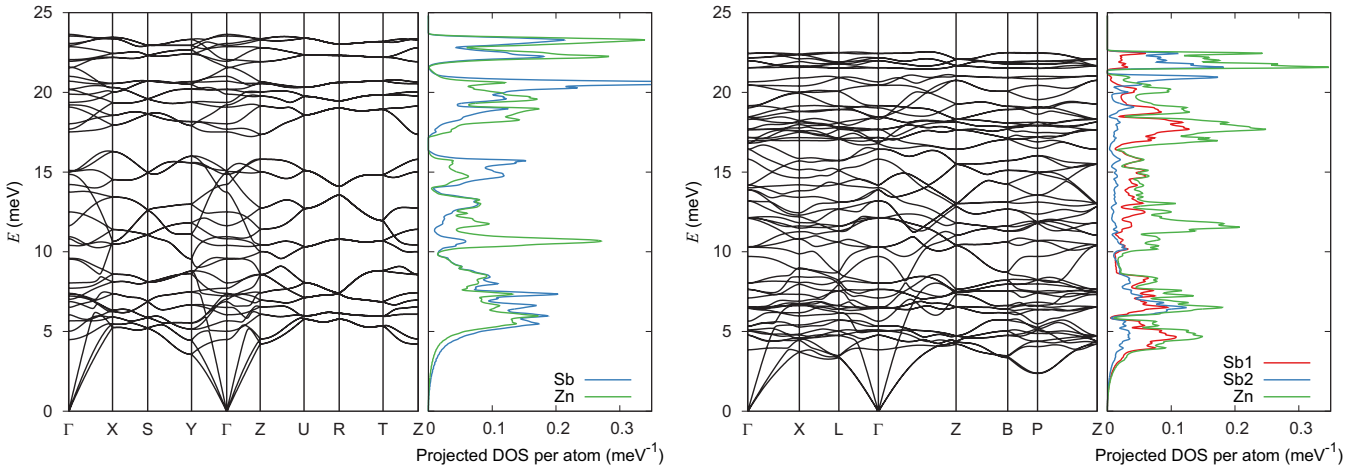

FIG. 6. (Color online) Phonon dispersion relations, and pure and weighted DOS for (a) ZnSb and (b) Zn_6Sb_5.

to note how the heat carrying phonons have a shorter MFP than in ZnSb, which would make the effect of nanostructuring smaller. It is also seen how the vacancies lower the contribution from the short MFP phonons, whereby the relative influence of nanostructuring is increased.

B. Origin of the low thermal conductivity

The calculated phonon dispersion relations and projected density of states (DOS) for ZnSb and Zn_6Sb_5 are shown in Fig. 6. Both structures have low-lying optical branches between 4 and 8 meV. In Table III the frequencies of the Raman-active modes are listed and compared to the experimentally observed peak energies [49]. The general agreement is similar to what is found for the ZnSb structure [14] and reasonable when taking into account the overestimated unit-cell volume, and resulting underestimated peak energies, obtained when using the PBE functional. This is also seen in the average speed of sound for Zn_6Sb_5, which is underestimated (Table I), compared to the experimental value of 2310 m/s [1]. Significant Zn-vibrational contributions are found for the low energy modes, and we found the Sb1 atoms to have a larger contribution than the Sb2 atoms. We also investigated the relative contributions of Zn and Sb vibrations to the individual eigenstates in the Brillouin zone, and in all cases found Zn contributions above 40%. This would disagree with the analysis by Schweika *et al.*, who estimated that in Zn_4Sb_3, these optical branches originated from Sb-Sb dumbbell rattling [21], but it aligns well with the conclusions drawn by Jund *et al.* [14]. Because of the high mobility of Zn in Zn_4Sb_3 [50], we would expect the Zn atoms to be loosely bound in this compound. The same is, apparently, true in ZnSb, since we also found soft Zn modes in ZnSb, which agrees well with our earlier observation of a low formation energy of Zn vacancies [15]. We would argue that the loose binding of the Zn atoms makes it impossible for the antimony dumbbells to rattle independently.

The low thermal conductivity of the Zn-Sb compounds is quantified by $(\omega^2\tau_M)$ and $\overline{(v/\omega)^2}$ [Eq. (14)] in Table I. Comparing the two compounds ZnTe and ZnSb, the thermal conductivity of ZnTe is about four times larger both

TABLE III. Energies of the Raman-active modes in meV. The experimental values are taken from Ref. [49].

PBE		
A_{1g}	E_g	Expt.
	4.76	
	6.46	
7.10	8.03	
	10.29	11.54
12.14	12.13	13.52
	13.19	15.38
	14.19	
16.79	17.66	18.98
18.45	19.16	21.22
20.44	21.55	22.49
	22.17	

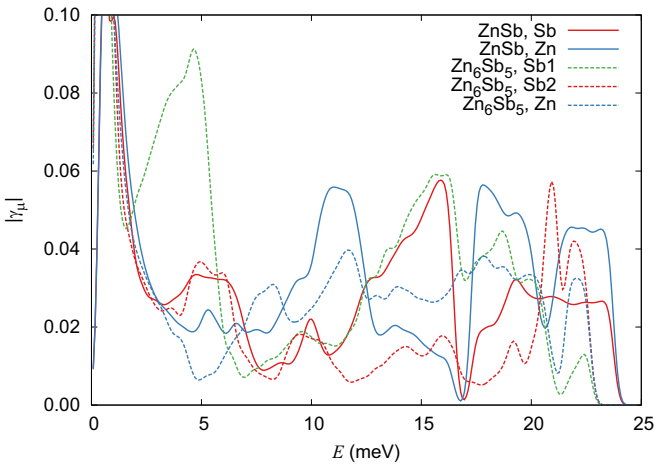

FIG. 7. (Color online) Root mean square of the mode Grüneisen parameters for ZnSb and Zn_6Sb_5.

experimentally and in the model. This is mainly due to a shorter relaxation time in ZnSb, whereas the velocity term $\overline{(v/\omega)^2}$ accounts for about one-third of the reduction. Comparing the 6:5 zinc antimonide to the 1:1, there is a drop of thermal conductivity by almost a factor 8, again in good agreement with experiment. It is seen that this is mainly due to a large decrease in $(\omega^2\tau_M)$. Table I shows that this decrease can almost entirely be attributed to the increase in the squared Grüneisen parameter of the acoustic bands $\tilde{\gamma}^2$ [Eq. (12)]. The very low

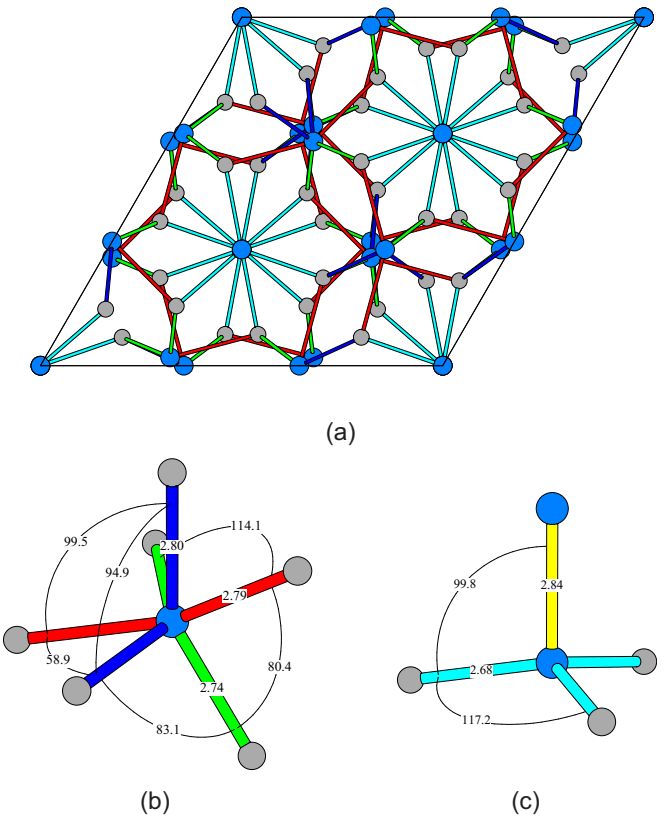

FIG. 8. (Color online) (a) Structure of the Zn_6Sb_5 structure used to model the 4:3 phase. (b) and (c) show the coordination of the Sb1 and Sb2 atoms, respectively.

thermal thermal conductivity in the 6:5 or 4:3 phase is thus due to a strong increase in the anharmonicity.

In Fig. 7, we introduce an atom projected contributions Grüneisen DOS

$$\gamma_\mu^2(\omega) = \left(\frac{V}{2\omega^2}\right)^2 \sum_i \int \left|\langle \phi_{\mu i\mathbf{q}} | \frac{\partial D}{\partial V} | e_{i\mathbf{q}} \rangle\right|^2 \delta(\omega - \omega_{i\mathbf{q}}) \frac{d\mathbf{q}}{8\pi^3}, \tag{24}$$

where $\phi_{\mu i\mathbf{q}}$ is a version of the eigenvector containing only nonzero elements on those entries which are related to the investigated atom μ. It is seen that the Zn and Sb2 atoms in Zn_6Sb_5 contribute to the Grüneisen parameter in a very similar way as those in the ZnSb, which is understandable by comparing the 6:5 structure (Fig. 8) to that of ZnSb (see Fig. 2 in Ref. [9]). The coordinations of atoms Zn and Sb2 are very similar to those in ZnSb. Both structures have Sb-Sb dumbbells with interatomic distances around 2.8 Å, where the Sb2 atoms furthermore coordinate to three Zn atoms. The Sb1 atoms coordinate a prism of six Zn nearest neighbors and are not involved in a Sb-Sb dumbbell. It is interesting to note how the large $\tilde{\gamma}^2$ is directly related to the Sb1 atoms (Fig. 7), which have no equivalent in the 1:1 structure. This provides a clear indication that the very low thermal conductivity of the Zn_4Sb_3 and its model 6:5 phase is directly related to a strongly anharmonic potential and local environment of the Sb1 atoms [Fig. 8(b)].

V. CONCLUSION

We have introduced a model to calculate the lattice thermal conductivity based on *ab initio* calculated phonon dispersions. The model has been found to give results in reasonable quantitative agreement with experiment and correctly predict the relative magnitudes of thermal conductivities in a number of semiconductor structures. The model is used to rationalize the relatively large effect of nanostructuring on the thermal conductivity of the zinc antimonides in terms of the mean free paths of the heat carrying phonons.

Low-lying optical modes involving both Zn and Sb vibrations are found in both ZnSb and Zn_6Sb_5, strongly questioning dumbbell rattling. Furthermore, in agreement with experiment, we found the thermal conductivity of Zn_6Sb_5 to be approximately eight times lower than in ZnSb. A mechanism for the very low thermal conductivity observed in Zn_4Sb_3 has been identified and traced to the anharmonic motion of the Sb1 atoms which coordinate only Zn atoms.

Since the 6:5 structure is an ordered model of the disordered 4:3 phase, disorder is not necessary to explain the low thermal conductivity of the disordered phase. The low thermal conductivity thus seems to be an inherent feature of these structures. However, it is also clear that disorder on the zinc lattice further lowers the thermal conductivity in the experimental phases.

ACKNOWLEDGMENTS

This work was supported by the Danish National Research Foundation (Center for Materials Crystallography, DNRF93), the Danish Strategic Research Council (Centre for Energy Materials), and the Danish Center for Scientific Computing. G.K.H.M. acknowledges financial support through ThyssenKrupp AG, Bayer MaterialScience AG, Salzgitter Mannesmann Forschung GmbH, Robert Bosch GmbH, Benteler Stahl/Rohr GmbH, Bayer Technology Services GmbH and the state of North-Rhine Westphalia, as well as the European Commission in the framework of the European Regional Development Fund (ERDF).

[1] T. Caillat, J. P. Fleurial, and A. Borshchevsky, J. Phys. Chem. Solids **58**, 1119 (1997).
[2] B. L. Pedersen and B. B. Iversen, Appl. Phys. Lett. **92**, 161907 (2008).
[3] B. L. Pedersen, H. Yin, H. Birkedal, M. Nygren, and B. B. Iversen, Chem. Mater. **22**, 2375 (2010).
[4] H. Yin and B. B. Iversen, Sci. Adv. Mater. **3**, 592 (2011).
[5] Y. Mozharivskyj, Y. Janssen, J. L. Harringa, A. Kracher, A. O. Tsokol, and G. J. Miller, Chem. Mater. **18**, 822 (2006).
[6] H. Yin, M. Christensen, B. L. Pedersen, E. Nishibori, S. Aoyagi, and B. B. Iversen, J. Electron. Mater. **39**, 1957 (2010).
[7] C. Okamura, T. Ueda, and K. Hasezaki, Mater. Trans. **51**, 860 (2010).
[8] P. H. M. Böttger, K. Valset, S. Deledda, and T. G. Finstad, J. Electron. Mater. **39**, 1583 (2010).
[9] L. Bjerg, G. K. H. Madsen, and B. B. Iversen, Chem. Mater. **23**, 3907 (2011).
[10] D. Benson, O. F. Sankey, and U. Häussermann, Phys. Rev. B **84**, 125211 (2011).
[11] P. H. M. Böttger, G. S. Pomrehn, G. J. Snyder, and T. G. Finstad, Phys. Status Solidi A **208**, 2753 (2011).
[12] K. Valset, P. H. M. Böttger, J. Taftø, and T. G. Finstad, J. Appl. Phys. **111**, 023703 (2012).
[13] X. Song, P. H. M. Böttger, O. B. Karlsen, T. G. Finstad, and J. Taftø, Phys. Scr. **T148**, 014001 (2012).
[14] P. Jund, R. Viennois, X. Tao, K. Niedziolka, and J.-C. Tedenac, Phys. Rev. B **85**, 224105 (2012).
[15] L. Bjerg, G. K. H. Madsen, and B. B. Iversen, Chem. Mater. **24**, 2111 (2012).
[16] D. Eklöf, A. Fischer, Y. Wu, E.-W. Scheidt, W. Scherer, and U. Häussermann, J. Mater. Chem. A **1**, 1407 (2013).
[17] P. J. Shaver and J. Blair, Phys. Rev. **141**, 649 (1966).
[18] G. J. Snyder, M. Christensen, E. Nishibori, T. Caillat, and B. B. Iversen, Nat. Mater. **3**, 458 (2004).
[19] W. Chen and J. Li, Appl. Phys. Lett. **98**, 241901 (2011).
[20] G. Li, Y. Li, L. Liu, Q. Zhang, and P. Zhai, Mater. Res. Bull. **47**, 3558 (2012).
[21] W. Schweika, R. P. Hermann, M. Prager, J. Perßon, and V. Keppens, Phys. Rev. Lett. **99**, 125501 (2007).
[22] A. Ward and D. A. Broido, Phys. Rev. B **81**, 085205 (2010).
[23] L. Lindsay, D. A. Broido, and T. L. Reinecke, Phys. Rev. Lett. **111**, 025901 (2013).

[24] G. A. Slack, in *Solid State Physics*, edited by F. S. Henry Ehrenreich and D. Turnbull (Academic, New York, 1979), Vol. 34, pp. 1–71.
[25] E. J. Skoug and D. T. Morelli, Phys. Rev. Lett. **107**, 235901 (2011).
[26] Y. Zhang, E. Skoug, J. Cain, V. Ozoliņš, D. Morelli, and C. Wolverton, Phys. Rev. B **85**, 054306 (2012).
[27] G. A. Slack and S. Galginaitis, Phys. Rev. **133**, A253 (1964).
[28] D. T. Morelli, J. P. Heremans, and G. A. Slack, Phys. Rev. B **66**, 195304 (2002).
[29] G. Leibfried and E. Schlömann, Nachr. Akad. Wiss. Göettingen, Math.-Phys., Kl. 2A: Math.-Phys.-Chem. Abt. **4**, 71 (1954).
[30] C. L. Julian, Phys. Rev. **137**, A128 (1965).
[31] K. Esfarjani, G. Chen, and H. T. Stokes, Phys. Rev. B **84**, 085204 (2011).
[32] W. Li, L. Lindsay, D. A. Broido, D. A. Stewart, and N. Mingo, Phys. Rev. B **86**, 174307 (2012).
[33] R. Kremer, K. Graf, M. Cardona, G. Devyatykh, A. Gusev, A. Gibin, A. Inyushkin, A. Taldenkov, and H.-J. Pohl, Solid State Commun. **131**, 499 (2004).
[34] G. A. Slack, Phys. Rev. B **6**, 3791 (1972).
[35] B. L. Pedersen, H. Birkedal, B. B. Iversen, M. Nygren, and P. T. Frederiksen, Appl. Phys. Lett. **89**, 242108 (2006).
[36] S. Bhattacharya, R. P. Hermann, V. Keppens, T. M. Tritt, and G. J. Snyder, Phys. Rev. B **74**, 134108 (2006).
[37] G. Kresse and J. Hafner, Phys. Rev. B **47**, 558 (1993).
[38] G. Kresse and J. Furthmüller, Phys. Rev. B **54**, 11169 (1996).
[39] J. P. Perdew, K. Burke, and M. Ernzerhof, Phys. Rev. Lett. **77**, 3865 (1996).
[40] P. E. Blöchl, Phys. Rev. B **50**, 17953 (1994).
[41] G. Kresse and D. Joubert, Phys. Rev. B **59**, 1758 (1999).
[42] A. Togo, F. Oba, and I. Tanaka, Phys. Rev. B **78**, 134106 (2008).
[43] P. G. Klemens, in *Kältephysik I/Low Temperature Physics I*, Handbuch der Physik/Encyclopedia of Physics (Springer-Verlag, Berlin, 1956), pp. 198–281.
[44] C. A. Ratsifaritana and P. G. Klemens, Int. J. Thermophys. **8**, 737 (1987).
[45] J. Nylén, M. Andersson, S. Lidin, and U. Häussermann, J. Am. Chem. Soc. **126**, 16306 (2004).
[46] Y. Wu, J. Nylén, C. Naseyowma, N. Newman, F. J. Garcia-Garcia, and U. Häussermann, Chem. Mater. **21**, 151 (2009).
[47] T. Dasgupta, C. Stiewe, L. Boettcher, R. Hassdorf, H. Yin, B. Iversen, and E. Mueller, J. Mater. Res. **26**, 1925 (2011).
[48] E. S. Toberer, P. Rauwel, S. Gariel, J. Taftø, and G. Jeffrey Snyder, J. Mater. Chem. **20**, 9877 (2010).
[49] R. Viennois, M.-C. Record, V. Izard, and J.-C. Tedenac, J. Alloys Compd. **440**, L22 (2007).
[50] E. Chalfin, H. Lu, and R. Dieckmann, Solid State Ionics **178**, 447 (2007).